Long-lasting intracontinental strike-slip faulting; new evidence from the Karakorum shear zone in the Himalayas.

Running head: **Long lasting activity of the Karakorum fault.**

P.H. Leloup[1], E. Boutonnet[1], W.J. Davis[2], K. Hattori[3].

1 L.S.T. UMR CNRS 5570, Université Lyon 1, France.
tel: [33] (0)4 72 44 62 38 ; fax: [33] (0)4 72 44 85 93 ; Email: herve.leloup@univ-lyon1.fr
2 ESS/GSC-CNCB/GSC-CC/GEOCHRON, Geological Survey of Canada.
3 Department of Earth Sciences, University of Ottawa, Canada.

Abstract

Zircon crystallization ages for a syntectonic granite and an associated dyke along the Tangtse strand of the Karakorum fault are of 18.5 ±0.2 Ma and 18.6±0.2 Ma, respectively. A dyke crosscutting the foliation in the Karakorum shear zone yield an age of 16.0 ± 0.6 Ma. These data show that the Karakorum shear zone was associated with significant granitic magmatism and was active before 16 Ma, since at least ~18.5 Ma. Considering other data along the Karakorum fault, the fault is most likely active since ~22.7 to 25 Ma at a rate of 8 to 13 mm/yr. This study conducted in the frontal part of the Himalayan orogen shows that large continental strike-slip faults can be linked with magmatism, and be stable for more than 20 Ma, even in the hottest part of orogens where strain localisation is supposed to be minimum.

Introduction

The rate and lifespan of intra-continental strike-slip faults is the subject of a long-standing debate. Some have suggested that such faults play a major role in the continental deformation (e.g., Tapponnier et al., 1986; Tapponnier et al., 2001), whereas others consider such faults as transient features accommodating limited deformation (e.g., England and Houseman, 1986). In the India / Eurasia collision zone this debate has mostly focussed on the late Holocene deformation rates along the main strike-slip faults, with some advocating for fast strike-slip rates (e.g., Chevalier et al., 2005; Mériaux et al., 2005) and others for nearly continuous deformation with minor faulting (e.g., Wallace et al., 2004; Wright et al., 2004; Zhang et al., 2004). A complementary approach to the problem is to discuss the life span, total amount of motion, and lithospheric or crustal nature of such faults over longer time scales of several millions years. To this respect, the nature, life span and offset of the Karakorum shear zone (Ksz) (Fig. 1a), have been lively discussed (e.g., Lacassin et al., 2004b). A related discussion stands on the ability or not, of these faults to produce and /or channel melts towards the surface (e.g., Hutton and Reavy, 1992; Leloup et al., 1999; Paterson and Schmidt, 1999).

The Karakorum Fault, is a more than 900km long strike-slip faults bounding Tibet to the SE (KF; Fig. 1a; Fig. 2a). It has been suggested that the KF is active since ~ 23 Ma with synkinematic magmatism occurring at that time in the North Ayilari range (NA in Fig. 2a) (Lacassin et al., 2004a; Valli et al., 2008). On the other hand, Phillips et al. (2004) proposed that 200 km away along strike of the fault near Tangtse (T in Fig. 2a), deformation postdates magmatism, starting after 15.7 Ma and lasting less than 2 Ma. This view, of a recent and short-

lived ductile deformation, that appears to have been widely accepted (Ravikant, 2006; Phillips and Searle, 2007; Rutter et al., 2007; Bhutani et al., 2009; Streule et al., 2009; Wang et al., 2009) has important bearings on the continental collision history and mechanics. Here we present data demonstrating that right-lateral deformation, that is still active today, started more than 18 Ma ago near Tangtse, and suggesting that there are close spatial and temporal relationships between strike-slip shearing and magmatism.

The Karakorum shear zone at Tangtse, relationships between magmatism and deformation.

In Ladakh, the main geological units trend WNW-ESE and are deflected and offset by the NW-SE right-lateral KF (Fig. 2a). The 120 km offset of the Indus River across the fault (Gaudemer et al., 1989) (Fig. 2a) most likely corresponds to the fault motion since 16 to 12 Ma ago (Valli et al., 2007). Correlations of geological units across the KF are not well established and the total offset has been debated, with estimates ranging from no offset (Jain and Singh, 2008) to 1000km (Peltzer and Tapponnier, 1988). Searle et al. (1998) proposed a maximum offset of 120–150 km by correlating the Baltoro and Tangtse granites (Fig. 2a). However, this correlation, if correct, would only provide a minimum offset as the 15.55±0.74 Ma old (Phillips et al., 2004) Tangtse granite is located between the two strands of the KFZ and postdate the KF initiation (This study). The large-scale warping of the Lower Cretaceous Shyok – Shiquanhe suture zone, the Cenozoic Indus – Tsangpo suture zone, and the Mesozoic Ladakh – Gangdese Mesozoic calc-alkaline batholith suggests an offset of 200 (Ratschbacher et al., 1994) to 240 km (Valli et al., 2008) (offset on Fig. 2a).

Near Tangtse (T, Fig. 2a), deformed plutonic, migmatitic and metamorphic rocks including mylonites outcrop in the Pangong range (Fig. 1b). They exhibit a foliation trending N131°, 84° SE on average with a stretching lineation dipping ~15° to the NW (Fig. 1b). These rocks correspond to the ~8 km right-lateral Ksz (e.g., Searle et al., 1998; Rolland and Pêcher, 2001; Phillips and Searle, 2007; Rolland et al., 2009), framed to the SW and NE by the Tangtse and the Muglib mylonitic strands (Fig. 1b). Morphological evidence indicates active right-lateral faulting along the Muglib strand (Brown et al., 2002). Note that the various authors give different names to the geologic formations. We use the names given on Fig. 1.

Mylonitic marbles, calcsilicates and orthogneiss outcrop on the Tangtse strand of the Ksz, around the Tangtse monastery (Fig. 1b). There, Phillips et al. (2004) obtained U/Pb ID-TIMS zircon and Monazite ages of 15.63±0.52 Ma from a mylonitised leucocratic dyke (sample

P11; Table A1; Fig. 1b) and 13.74±0.29 Ma from a cross-cutting dyke (sample P8). They concluded that ductile deformation started after ~ 15.6 Ma and ceased prior to ~ 13.7 Ma. We noted that the cross-cutting dyke is not ~5 km long as depicted by Searle and Phillips (2007), but less than 5 m with two asymmetric tails compatible with right-lateral ductile deformation. The fact that the dyke crosscut the foliation formed by right-lateral shear but is also affected by that deformation implies that it is a synkinematic intrusion. Sample LA60 was taken from another horizontal leucocratic dyke crosscutting the foliation trending N116 (Fig. 3f). Its crystallization age will thus provide a minimum age for the onset of ductile deformation.

The South Tangtse granite (STG) outcropping at the southern margin of the Ksz (Fg. 1b) shows a strong deformation gradient from the SW to the NE (Fig. 3). The STG contains large crystals of K-feldspar, quartz and biotite, and is cut by leucocratic dykes. Both granite and dykes are totally undeformed ~ 400 m south of the Tangtse stand of the Ksz. Towards the Ksz, a faint steep magmatic foliation trending N130 to N105 is defined by the preferred orientation of large K-feldspar crystals and mafic enclaves (Fig. 3c, d). Farther to the NE, both granite and leucocratic dykes show a progressively stronger foliation, which becomes mylonitic trending N125, 70 SW (Fig. 3e), with a lineation dipping ~12° to the NW and right-lateral shear criteria. NE of this outcrop all rocks are strongly deformed and locally contain thin mafic layers with a foliation trending N110 to N130 and lineation close to horizontal (Fig. 1c). The evidence presented in the STG including the progressive deformation increase towards the Ksz and the occurrence of a magmatic foliation parallel to the Ksz and to the mylonitic foliation, is diagnostic of a syntectonic intrusion that will provide a minimum age for deformation.

Emplacement ages of syntectonic granitoids in the Tangtse strand of the Karakorum shear zone.

Zircon grains from samples LA20 (leucocratic dyke) and LA21 (granite) of the undeformed part of the STG, as well as from sample LA60 were dated with the SHRIMP II at the Geological Survey of Canada during two sessions. Analytical procedures and detailed analysis of the data are given in appendix A1, a summary of the results in Table 1 and detailed results in Table A2.

Zircons from sample LA21b show typical magmatic growth zoning in cathodoluminescent images, with some grains showing high-U cores and the evidence of resorption before re-growth (Fig. 4b). One core yield an age of 310±5 Ma (Carboniferous), while 11 rim spots yield a lower intercept age of 18.5±0.2 Ma (MSWD = 2.07, common Pb

anchored upper intercept) (Fig. 4b), which we consider as the best age approximation for these rims, and for the granite final crystallization.

Zircon from an undeformed dyke (LA20) collected at the same location as LA21b yielded very similar results. The zircon grains are euhedral, well zoned, with rare cores that are partially resorbed (Fig. 4a). One core has an age of 25.6±0.3 Ma, while 17 rim analyses define a regression line in a Tera-Wasserburg plot with a lower intercept at 18.61±0.25 Ma (Fig. 4a). The results suggest the presence of a ~26 Ma inheritance and final magma crystallization at ~18.6 Ma, which is synchronous with the surrounding granite.

Zircons extracted from Sample LA60 are strongly metamict with exsolved uraninite (Fig. 4c), and show very high U contents from 2,900 to 12,700 ppm. For zircon with U contents > 2000 ppm ion probe analytical matrix effect may yield inaccurate old ages if uncorrected (Williams and Hergt, 2000). Correction of such effect yields an age of 16.0 ± 0.6 Ma (6 meas., MSWD = 2.6 - 6 grains) (Fig. 4c). This age is, interpreted as the time of crystallisation of the late dyke.

Deformation timing in the Karakorum shear zone and geodynamic consequences.

Lower Miocene granitic rocks of the Ksz both in Tangtse and Ayilari span in age from ~25 to ~13 Ma, and have been interpreted to be syntectonic to right-lateral shearing (Valli et al., 2008; Weinberg and Mark, 2008; Reichardt et al., 2010) (Fig. 1b, Appendix A2, Table A1). Leucogranites of the Pangong range have been interpreted as the product of synkinematic water-fluxed melting of the Late Cretaceous granodiorites and of the Tangtse meta-sedimentary rocks (Reichardt et al., 2010). This interpretation is contested by some authors that consider that all magmatic rocks within the Ksz, unless few isolated dykes, predate deformation (e.g. Phillips et al., 2004; Searle and Phillips, 2004) and that ductile deformation occurred at temperature below solidus (Phillips and Searle, 2007). In that interpretation, right-lateral shear was mostly restrained between 15.7 and 13.7 Ma and the KF is a transient structure. However, our study shows clear evidences that the 18.5 Ma South Tangtse granite is syntectonic, and that strike-slip deformation started prior to 16 Ma in the Tangtse strand. Within the shear zone, part of the evidence for high-temperature deformation has probably been obscured by overprinting of low temperature structures formed during cooling, as temperature dropped to ~400°C at ~13 Ma (Dunlap et al., 1998) while right-lateral shear pursued. Such evidence has been preserved in the South Tangtse granite because it occurs at the margin of the main deformation zone (Fig. 1b).

The age of syntectonic intrusions imply that the KF initiated prior to 22.7±0.1 Ma in the North Ayilari (sample C32, Valli et al., 2007) and 18.5±0.2 near Tangtse (STG; this study) (Fig. 2b). As the fault is still active this ages yield an integrated slip rate of 8.8 to 13 mm/yr along the central section of KF. At the southern extremity of the main KF strand (SA, Fig. 2a), Murphy et al. (2000), suggested that the South Kailash thrust (SKT on Fig. 2a) was offset 66 ± 5.5 km by the KF. The ~19 - 13 Ma age of that thrust, based on a single K-feldspar Ar-Ar thermal history (Yin et al., 1999), was taken to imply that the KF would be younger than 13 Ma at this location (Fig. 2b) with a slip rate ≥ 5.5±0.4 mm/yr. If this piercing point is correct it would imply a very slow propagation of the fault toward the South (Fig. 2b) and an abrupt decrease of the fault motion toward the Gurla Mandhata (GM), or a slow-down from ~14 to ~4 mm/yr at ~13 Ma. Alternatively, assuming all Miocene intrusions along the KF to be syntectonic would imply a slightly older initiation age, a lower integrated slip-rate (8 – 10 mm/yr), and a faster fault propagation (Fig. 2b) (Valli et al., 2008).

The Ksz appears a good pathway for magma produced deeper in the crust to ascend (e.g., Valli et al., 2008; Weinberg and Mark, 2008; Reichardt et al., 2010). Leech (2008) even proposed that the Ksz acted as a barrier collecting all magmas flowing at mid-crustal level from North Tibet towards the south in the framework of the lower crustal channel flow model. This hypothesis would explain why Himalayan granites are fewer and older west of the GM interpreted as the KF SE tip (Fig. 2a). This hypothesis appears sustained by the fact that the STDS, interpreted as the upper bound of the channel, stopped earlier west of the GM than further east. However, this stop occurs at ~17 Ma, thus ~8 Ma after the initiation of magmatism in the Ksz (Fig. 2b) (Leloup et al., 2010) and it is difficult to link the two events. Alternatively, ductile shear heating in the upper mantle could have triggered partial melting in the lower crust. However numerical simulations suggest that for fault rates of ~10 mm/yr, comparable to what we propose for the KF, it could be the case only for unlikely circumstances: very stiff upper mantle and very fertile lower crust (Leloup et al., 1999). Therefore, we suggest that crustal melts collected by the Ksz resulted from high heat flow resulting from crustal thickening (e.g., Huerta et al., 1998), and /or heat advection following slab breakoff (Mahéo et al., 2009). Melting was probably enhanced by fluid circulation (Reichardt et al., 2010).

Large intracontinental strike-slip faults have long been proposed as major conduits collecting fluids and melts originated in the lower crust or the upper mantle (i.e., Hutton and Reavy, 1992; Leloup et al., 1999 and references therein). Within transpressive orogens such large strike-slip faults promote magmas and hot fluid ascent playing a major role in the crust

evolution (e.g., Hollister and Andronicos, 2006; Pirajno, 2010). Whatever the source of fluid, the upward fluid flow will increase the local thermal gradient, soften the rocks and promote strain localisation within the strike-slip shear zone. As a consequence strain localisation could be enhanced in strike-slip faults that thus could be stable through time and absorb large displacements, as long as boundary conditions do not change considerably. Our data confirm that this was the case for the KF during the last ~25 Ma even though it is located in frontal part of the orogen where the high thermal gradient is expected to promote diffuse deformation rather than strain localisation.

Acknowledgements.

Fieldwork was funded by the CNRS / INSU 3F program. L. Ratschbacher and an anonymous referee are thanked for their reviews. Organizers and participants to the 23rd HKT field excursion in Tangtse are thanked for stimulating discussions on the syntectonic, or not, nature of the granitoids within the Tangtse shear zone. B. Heulin of the French embassy in New Delhi is thanked for his help in sending back the samples.

Tables :

Table 1 U/Pb data summary for LA20, 21 and 60.

Figures captions :

Fig. 1 Structural map of the Karakorum shear zone in the Tangtse area

a) India – Eurasia collision main strike-slip faults: SF, Sagaing; RRF, Red River; XF, Xianshuihe; Ku, Kunlun; ATF, Althyntagh; KF, Karakorum. White arrows and black arrows respectively show active and past sense. Black frame corresponds to Fig. 2. **b)** Structural map of the Tangtse area. UTM 44 projection. **c)** Plot of foliations and lineations in the Tangtse shear zone, along the Tangtse gorge and in the south Tangtse granite (STG). Schmidt diagram, lower hemisphere.

Fig. 2 Geology along the KF and corresponding timing constraints

a) Black framed area of Fig. 1a. SA; South Ayilari (Namru); NA, North Ayilari; T, Tangtse; D, Darbuk; S, Satti,; P, Panamik; Za, Zanskar; Gw, Garwal; GM, Gurla Mandata; LP, Leo Pargil; SKT, South Kailash thrust. Geological units drawn from bibliography and Landsat imagery interpretation. MKT: Main Karakorum thrust corresponding to the Shyok suture zone, MMT: Main Mantle Thrust corresponding to the Indus suture zone **b)** Timing constraints plotted along the fault. U/Pb data and corresponding references are reported in Table A1. Red frames indicate syntectonic granitoids. Timing constraints for the STDS from Leloup et al. (2010).

Fig. 3 Detailed geological cross section of the Tangtse strand of the Karakorum shear zone near Tangtse monastery.

a) Geological cross-section of Ksz Tangtse strand based on field observation. **b to f)** photographs of facies and structures along section. **b)** Undeformed South Tangtse granite (sample LA21) with an undeformed leucocratic dyke (sample LA20). **c)** Faint magmatic foliation (fm) defined by the preferred orientation of coarse-grained K-feldspar. A 5 cm wide compass as a scale. **d)** Magmatic foliation (fm) marked by the orientation of mafic enclaves. A hammer as a scale. **e)** Mylonitic orthogneiss and leucocratic dyke affected by right-lateral deformation (foliation trends N130 72S and lineation dips 10W). View from above, hammer peak gives scale. **f)** Horizontal crosscutting leucocratic dyke (sample LA60). Foliation (Fo) is outlined in black and trends ~N115.

Fig. 4. U/Pb zircon Shrimp II data for samples LA20, LA21b and LA60.

See data in Tables A2 & A3. **a&b)** LA20 & LA21b Tera-Wasserburg plots and corresponding regressions. Data error ellipses are at 1σ, grey and black for first and second session respectively. c) LA 60 plot for ^{297}Pb corrected ^{206}Pb/^{238}U ages vs ^{238}U/$^{96}Zr_2O$ and regression line indicating a single age of 16.0±0.6 Ma. Data point errors are 1σ. Insets are examples of cathodoluminescence images with corresponding ^{206}U/^{238} ages.

References :

Bhutani, R., Pande, K. and Venkatesan, T.R., 2009. 40Ar–39Ar dating of volcanic rocks of the Shyok suture zone in north–west trans-Himalaya: Implications for the postcollision evolution of the Shyok suture zone *Journal of Asian Earth Sciences*, 34, 168-177.

Brown, E.T., Bendick, R., Bourlès, D.L., et al., 2002. Slip rates of the Karakorum fault, Ladakh, India, determined using cosmic ray exposure dating of debris flows and moraines *Journal of Geophysical Research-Solid Earth*, 107.

Chevalier, M.-L., Ryerson, F.J., Tapponnier, P., et al., 2005. Slip-Rate Measurements on the Karakorum Fault May Imply Secular Variations in Fault Motion *Science*.

Dunlap, W.J., Weinberg, R.F. and Searle, M.P., 1998. Karakorum fault zone rocks cool in two phases *Journal of the Geological Society*, 155, 903-912.

England, P. and Houseman, G., 1986. Finite strain calculations of continental deformation, 2. comparison with the India-Asia collision zone *Journal of Geophysical Research*, 91, 3664-3676.

Gaudemer, Y., Tapponnier, P. and Turcotte, D.L., 1989. River offsets across active strike-slip faults *Annales Tectonicae*, 3, 55 – 76.

Hollister, L.S. and Andronicos, C.L., 2006. Formation of new continental crust in Western British Columbia during transpression and transtension *Earth and Planetary Science Letters*, 249, 29-38.

Huerta, A.D., Royden, L.H. and Hodges, K.V., 1998. The thermal structure of collisional orogens as a response to accretion, erosion, and radiogenic heating *Journal of Geophysical Research-Solid Earth*, 103, 15287–15302.

Hutton, D.H.W. and Reavy, R.J., 1992. Strike-slip tectonics and granitepetrogenesis *Tectonics*, 11, 960–967.

Jain, A.K. and Singh, S., 2008. Tectonics of the southern Asian Plate margin along the Karakoram Shear Zone: Constraints from field observations and U–Pb SHRIMP ages *Tectonophysics*, 451, 186–205.

Lacassin, R., Valli, F., Arnaud, N., et al., 2004a. Large-scale geometry, offset and kinematic evolution of the Karakorum fault, Tibet *Earth and Planetary Science Letters*, 219, 255-269.

Lacassin, R., Valli, F., Arnaud, N., et al., 2004b. Reply to Comment on large-scale geometry, offset and kinematic evolution of the Karakorum fault, TibetQ *Earth and Planetary Science Letters*, 229, 159– 163.

Leech, M.L., 2008. Does the Karakoram fault interrupt mid-crustal channel flow in the western Himalaya? *Earth and Planetary Science Letters*, 276, 314–322.

Leloup, P.H., Ricard, Y., Battaglia, J. and Lacassin, R., 1999. Shear heating in continental strike-slip shear zones: numerical modeling and case studies. *Geophysical Journal International*, 136, 19-40.

Mahéo, G., Blichert-Toft, J., Pin, C., et al., 2009. Partial Melting of Mantle and Crustal Sources beneath South Karakorum, Pakistan: Implications for the Miocene Geodynamic Evolution of the India-Asia Convergence Zone *Journal of Petrology*.

Mériaux, A.-S., Tapponnier, P., Ryerson, F.J., et al., 2005. The Aksay segment of the northern Altyn Tagh fault: Tectonic geomorphology, landscape evolution, and Holocene slip rate *Journal of Geophysical Research-Solid Earth*, 110, 32 PP.

Murphy, M.A., Yin, A., Kapp, P., et al., 2000. Southward propagation of the Karakoram fault system, Southwest Tibet; timing and magnitude of slip *Geology*, 28, 451 – 454.

Paterson, S.R. and Schmidt, K.L., 1999. Is there a close spatial relationship between faults and plutons? *Journal of Structural Geology*, 21, 1131-1142.

Peltzer, G. and Tapponnier, P., 1988. Formation and evolution of strike-slip faults, rifts, and basins during the India-Asia collision: An experimental approach *Journal of Geophysical Research-Solid Earth*, 93, 15,085 – 015,117.

Phillips, R.J., Parrish, R.R. and Searle, M.P., 2004. Age constraints on ductile deformation and long-term slip rates along the Karakoram fault zone, Ladakh *Earth and Planetary Science Letters*, 226, 305-319.

Phillips, R.J. and Searle, M.P., 2007. Macrostructural and microstructural architecture of the Karakoram fault: relationship between magmatism and strike-slip faulting *Tectonics*, 26.

Pirajno, F., 2010. Intracontinental strike-slip faults, associated magmatism, mineral systems and mantle dynamics: examples from NW China and Altay-Sayan (Siberia) *Journal of Geodynamics*, 50, 325-346.

Ratschbacher, L., Frisch, W., Liu, G. and Cheng, C.C., 1994. Distributed deformation in Southern and Western Tibet as result of the India-Asia collision *Journal of Geophysical Research-Solid Earth*, 99, 19,917 – 919,945.

Ravikant, V., 2006. Utility of Rb–Sr geochronology in constraining Miocene and Cretaceous events in the eastern Karakoram, Ladakh, India *Journal of Asian Earth Sciences*, 27, 534–543.

Reichardt, H., Weinberg, R.F., Andersson, U.B. and Fanning, M.C., 2010. Hybridization of granitic magmas in the source: The origin of the Karakoram Batholith, Ladakh, NW India *Lithos*, 116, 249-272.

Rolland, Y., Mahéo, G., Pêcher, A. and Villa, I.M., 2009. Syn-kinematic emplacement of the Pangong metamorphic and magmatic complex along the Karakorum Fault (N Ladakh) *Journal of Asian Earth Sciences*, 34, 10–25.

Rolland, Y. and Pêcher, A., 2001. The Pangong granulites of the Karakoram Fault (Western Tibet): vertical extrusion within a lithosphere-scale fault? *Comptes rendus de l'académie des sciences de Paris*, 332, 363–370.

Rutter, E.H., Faulkner, D.R., Brodie, K.H., et al., 2007. Rock deformation processes in the Karakorum fault zone, Eastern Karakoram, Ladakh, NW India *Journal of Structural Geology*, 29, 1315-1326.

Searle, M.P. and Phillips, R.J., 2004. A comment on Large-scale geometry, offset, and kinematic evolution of the Karakoram fault, Tibet Q by R. Lacassin et al. *Earth and Planetary Science Letters*, 219, 255–269.

Searle, M.P. and Phillips, R.J., 2007. Relationships between right-lateral shear along the Karakoram fault and metamorphism, magmatism, exhumation and uplift: evidence from the K2–Gasherbrum–Pangong ranges, north Pakistan and Ladakh *Journal of the Geological Society*, 164, 439–450.

Searle, M.P., Weinberg, R.F. and Dunlap, W.J., 1998. Transpressional tectonics along the Karakoram fault zone, northern Ladakh: constraints on Tibetan extrusion. In: *Continental Transpressional and Transtensional Tectonics* (R.E. Holdsworth, S.R. A. and J.F. Dewey eds).

Streule, M.J., Phillips, R. J., Searle, M.P., et al., 2009. Evolution and chronology of the Pangong Metamorphic Complex adjacent to the Karakoram Fault, Ladakh: constraints from thermobarometry, metamorphic modelling and U–Pb geochronology *Journal of the Geological Society*, 166, 919–932.

Tapponnier, P., Peltzer, G. and Armijo, R., 1986. On the mechanics of the collision between India and Asia. In: *Collision Tectonics* (M.P. Coward and A.C. Ries, eds). Geological Society, London.

Tapponnier, P., Zhiqin, X., Roger, F., et al., 2001. Oblique stepwise rise and growth of the Tibet plateau *Science*, 294, 1671-1677.

Valli, F., Arnaud, N., Leloup, P.H., et al., 2007. 20 million years of continuous deformation along the Karakorum fault, Western Tibet: a thermochronological analysis *Tectonics*, 26.

Valli, F., Leloup, P.H., Paquette, J.-L., et al., 2008. New U-Th/Pb constraints on timing of shearing and long-term slip-rate on the Karakorum fault *Tectonics*, 27.

Wallace, K., Yin, G. and Bilham, R., 2004. Inescapable slow slip on the Altyn Tagh fault *Geophysical Research Letters*, 31, 4 PP.

Wang, S., Fang, X., Lai, Q., et al., 2009. New radiometric dating constrains the time for initiation of the Karakorum fault zone (KFZ), SW Tibet *Tectonophysics*.

Weinberg, R.F. and Mark, G., 2008. Magma migration, folding, and disaggregation of migmatites in the Karakoram Shear Zone, Ladakh, NW India *Geological Society of America Bulletin*, 120, 994–1009.

Williams, I.S. and Hergt, J.M., 2000. U-Pb dating of tasmanian dolerites: a cautionary tale of SHRIMP analysis of high-U zircon. In: *New frontiers in Isotope Geoscience* (J.D. Woodhead, J.M. Hergt and W.P. Noble, eds), Lorne.

Wright, T.J., Parsons, B., England, P.C. and Fielding, E.J., 2004. InSAR Observations of Low Slip Rates on the Major Faults of Western Tibet *Science*, 305, 236-239.

Yin, A., Harrison, T.M., Murphy, M.A., et al., 1999. Tertiary deformation history of southeastern and southwestern Tibet during the Indo-Asian collision *Geological Society of America Bulletin*, 111, 1644 – 1664.

Zhang, P.-Z., Shen, Z., Wang, M., et al., 2004. Continuous deformation of the Tibetan Plateau from global positioning system data *Geology*, 32, 809-812.

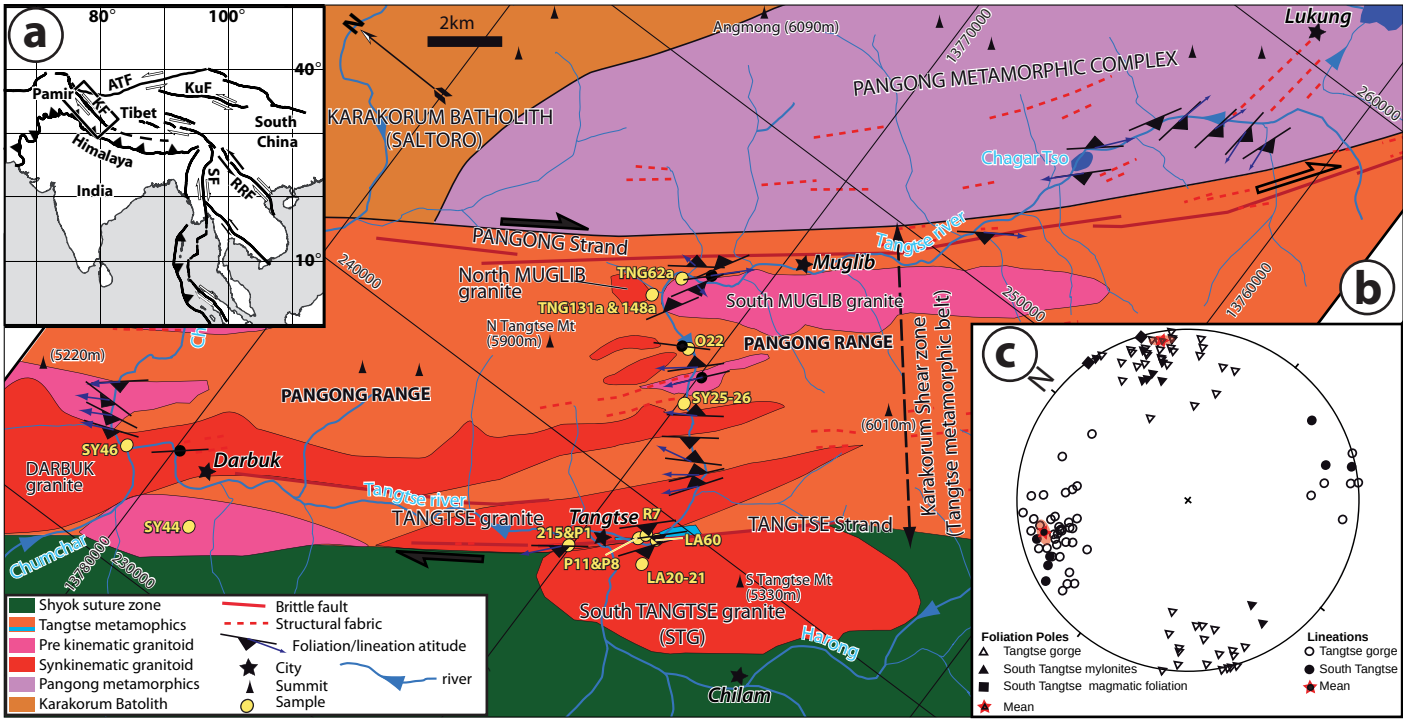
a
80°
100°
40°
10°
Pamir
ATF
KuF
KF
Tibet
South China
Himalaya
India
SF
RRF
2km
KARAKORUM BATHOLITH (SALTORO)
Angmong (6090m)
PANGONG METAMORPHIC COMPLEX
Lukung
Chagar Tso
PANGONG Strand
Tangtse river
Muglib
North MUGLIB granite
TNG62a
TNG131a & 148a
South MUGLIB granite
N Tangtse Mt (5900m)
O22
PANGONG RANGE
(5220m)
SY25-26
(6010m)
Karakorum Shear zone (Tangtse metamorphic belt)
SY46
Darbuk
DARBUK granite
Tangtse river
TANGTSE granite
Tangtse
R7
215&P1
LA60
TANGTSE Strand
SY44
Chumchar
P11&P8
LA20-21
S Tangtse Mt (5330m)
South TANGTSE granite (STG)
Harong
Chilam
240000
250000
260000
1377000
1376000
b
c
N
Foliation Poles
Tangtse gorge
South Tangtse mylonites
South Tangtse magmatic foliation
Mean
Lineations
Tangtse gorge
South Tangtse
Mean
Shyok suture zone
Tangtse metamophics
Pre kinematic granitoid
Synkinematic granitoid
Pangong metamorphics
Karakorum Batolith
Brittle fault
Structural fabric
Foliation/lineation atitude
City
Summit
Sample
river

Figure 1

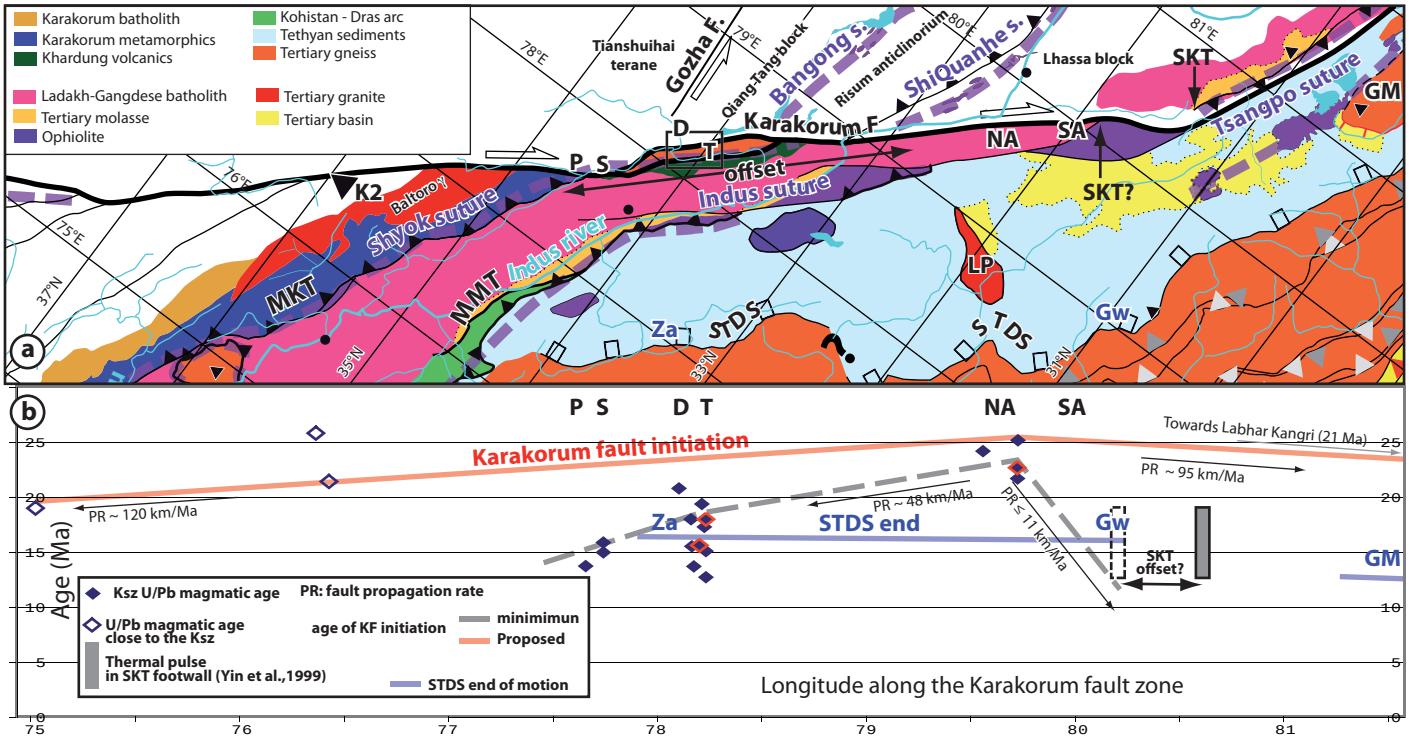
Karakorum batholith
Karakorum metamorphics
Khardung volcanics
Ladakh-Gangdese batholith
Tertiary molasse
Ophiolite
Kohistan - Dras arc
Tethyan sediments
Tertiary gneiss
Tertiary granite
Tertiary basin
a
Tianshuihai terane
Gozha F.
Qiang-Tang block
Bangong s.
Risum anticlinorium
ShiQuanhe s.
Lhassa block
SKT
GM
Tsangpo suture
Karakorum F
D
T
P
S
NA
SA
offset
Indus suture
SKT?
K2
Baltoro γ
Shyok suture
Indus river
MKT
MMT
LP
Za
STDS
Gw
78°E
79°E
80°E
81°E
75°E
76°E
37°N
35°N
33°N
31°N
b
P S
D T
NA SA
Towards Labhar Kangri (21 Ma)
Karakorum fault initiation
PR ~ 120 km/Ma
PR ~ 48 km/Ma
PR ~ 95 km/Ma
PR ≤ 11 km/Ma
STDS end
SKT offset?
Age (Ma)
Ksz U/Pb magmatic age
U/Pb magmatic age close to the Ksz
Thermal pulse in SKT footwall (Yin et al.,1999)
PR: fault propagation rate
age of KF initiation
minimimun
Proposed
STDS end of motion
Longitude along the Karakorum fault zone
0
5
10
15
20
25
75
76
77
78
79
80
81

Fig. 2

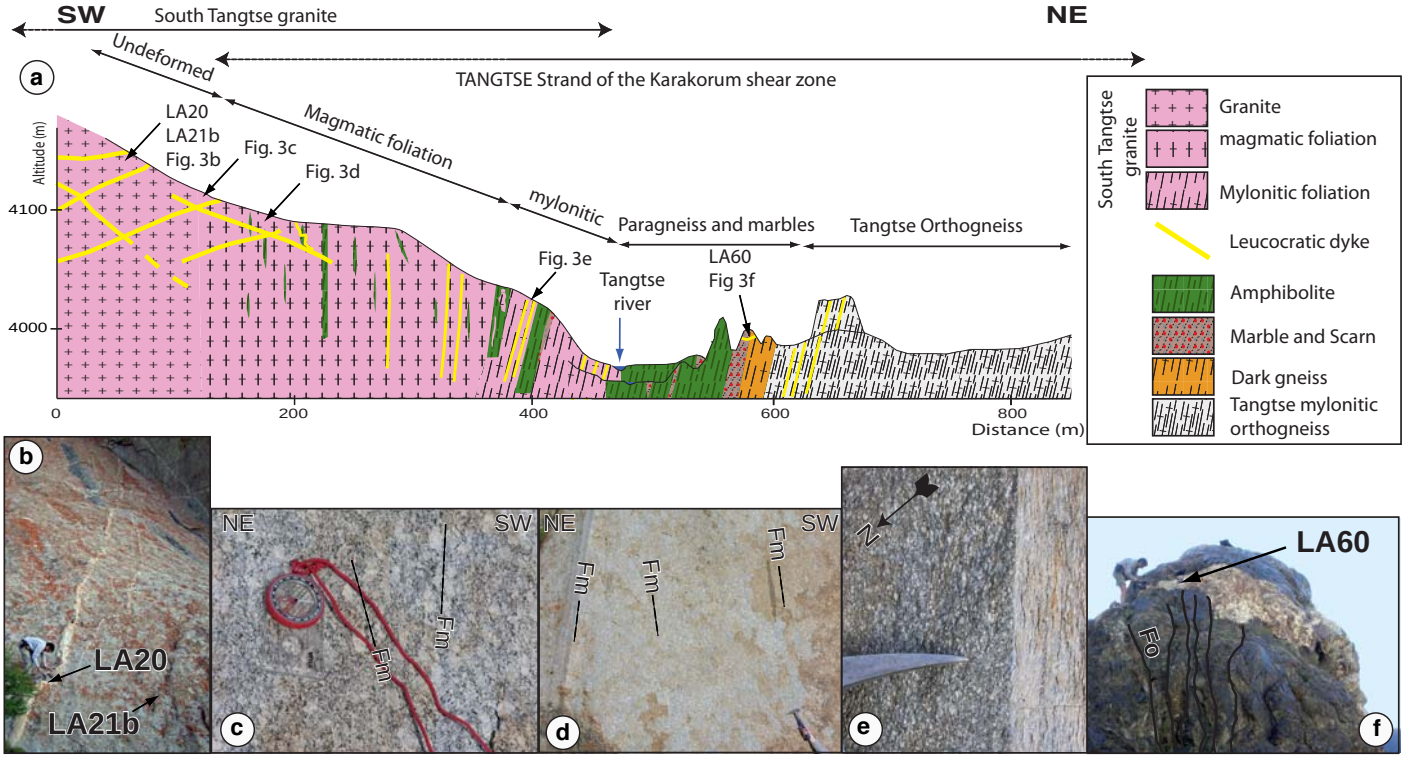
SW
South Tangtse granite
NE
a
Undeformed
TANGTSE Strand of the Karakorum shear zone
Magmatic foliation
mylonitic
LA20
LA21b
Fig. 3b
Fig. 3c
Fig. 3d
Fig. 3e
Tangtse river
LA60
Fig 3f
Paragneiss and marbles
Tangtse Orthogneiss
Altitude (m)
4100
4000
0
200
400
600
800
Distance (m)
South Tangtse granite
Granite
magmatic foliation
Mylonitic foliation
Leucocratic dyke
Amphibolite
Marble and Scarn
Dark gneiss
Tangtse mylonitic orthogneiss
b
LA20
LA21b
NE
SW
Fm
c
d
e
N
LA60
Fo
f

Fig. 3

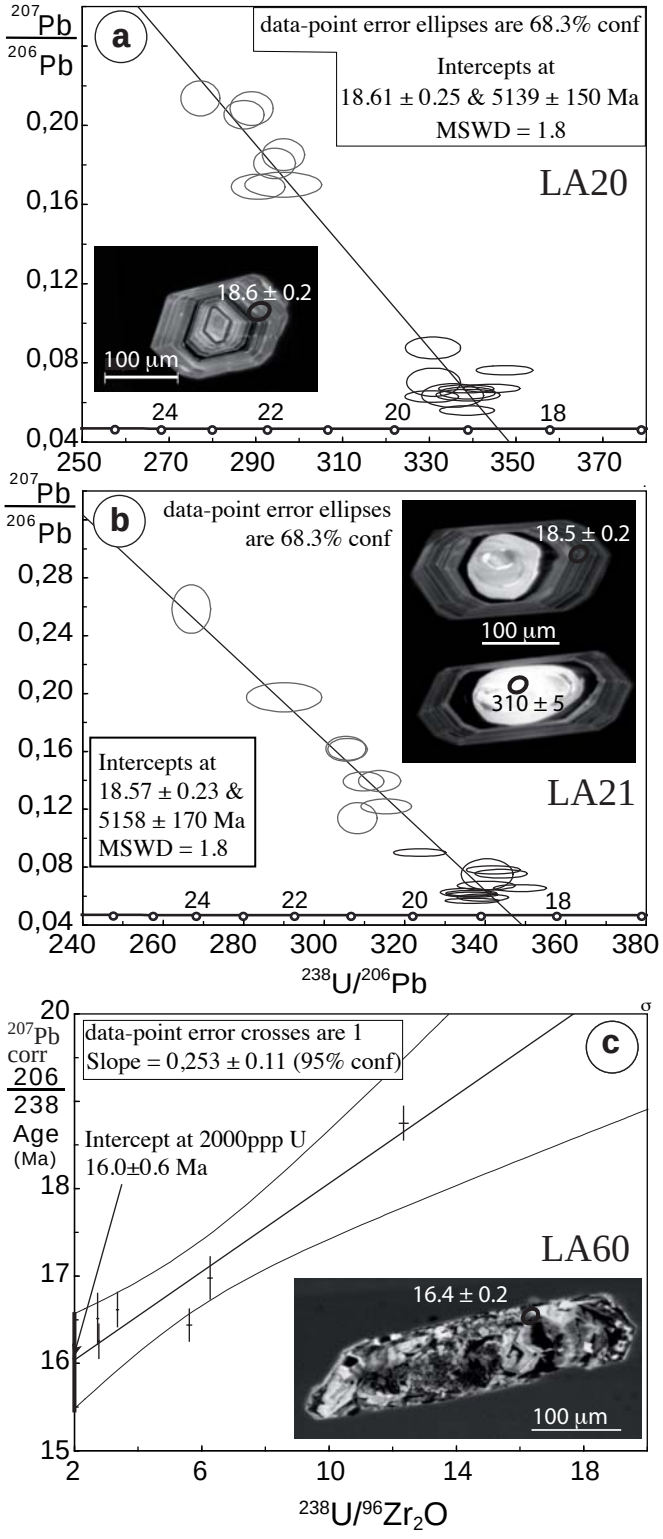
a
data-point error ellipses are 68.3% conf
Intercepts at
18.61 ± 0.25 & 5139 ± 150 Ma
MSWD = 1.8
LA20
18.6 ± 0.2
100 µm
b
data-point error ellipses
are 68.3% conf
18.5 ± 0.2
100 µm
310 ± 5
Intercepts at
18.57 ± 0.23 &
5158 ± 170 Ma
MSWD = 1.8
LA21
c
data-point error crosses are 1
Slope = 0,253 ± 0.11 (95% conf)
Intercept at 2000ppp U
16.0±0.6 Ma
LA60
16.4 ± 0.2
100 µm

Fig. 4

Site	Sample						Session	Average 206Pb/238U age 207 Pb corrected				Session	207Pb/206Pb vs 238U/206Pb (Tera-Wesserburg) age					interpretation
	Number	Rock type	Characteristics	Localisation (UTM. WGS84)				Age (Ma)	MSWD	Number of spots/ grains	Spots (crystal n°, border (b) or core (c))		Lower intercept (Ma)	Upper intercept (Ma)	MSWD	Number of spots/ grains	Common lead anchored	
				Zone	X	Y												
South Tangts granite	LA20	Leucocratic dike	undeformed	44	238815	3768161	2	**18.6 ± 0.2**	2.18	10/10	*1b, 2b, 5b, 10b, 11b, 14b, 18b, 19b, 20b, 21b*	1 & 2	18.6 ± 0.3	5139 ± 150	1.8	17/14	*no*	emplacement age
							1	**25.6 ± 0.3**	-	1/1	*17c*							inherited age
South Tangtse granite	LA21b	Granite	undeformed	44	238815	3768161	2	**18.5 ± 0.2**	2.07	11/11	*2b, 4b, 5b, 6b, 8b, 9b, 11b, 22b, 25b, 26b, 28b*	1 & 2	18.6 ± 0.2	5158 ± 170	1.8	19/19	*no*	emplacement age
							1	**310 ± 5**	-	1/1	*20c*							inherited age
								Age vs U(ppm) age										
								Intercept at 2000ppm (Ma)	MSWD	Number of spots/ grains	Spots (crystal n°/ border (b) or core (c))							
Tangtse strand	LA60	Leucocratic dike	cross cutting	44	239212	3768440	1	**16.0 ± 0.6**	2.6	6/6	*2b, 3b, 4b, 6b, 14b, 17b*							emplacement age

Table 1

Long-lasting intracontinental strike-slip faulting; new evidences from the Karakorum shear zone in the Himalayas.

Appendix.

A1 U/Pb dating methodology, analytical Techniques and samples data presentation.

SHRIMP analytical procedures followed those described by Stern (1997), with standards and U-Pb calibration methods following Stern and Amelin (2003). Briefly, zircons were cast in 2.5 cm diameter epoxy mounts (GSC IP531) along with fragments of the GSC laboratory standard zircon (z6266, with $^{206}Pb/^{238}U$ age = 559 Ma). The mid-sections of the zircons were exposed using 9, 6, and 1 μm diamond compound, and the internal features of the zircons (such as zoning, structures, alteration, etc.) were characterized in back-scattered electron mode (BSE) utilizing a Zeiss Evo 50 scanning electron microscrope. Mount surfaces were evaporatively coated with 10 nm of high purity Au. Analyses were conducted in two sessions using either an $^{16}O^-$ or $^{16}O_2^-$ primary beam, projected onto the zircons at 10 kV. The sputtered area used for analysis was ca. 15 μm in diameter (ca. 20 μm for session 2) with a beam current of ca. 15 nA. The count rates at ten masses including background were sequentially measured over 5 scans with a single electron multiplier and a pulse counting system with deadtime of 8 ns. Off-line data processing was accomplished using Squid 2.22.08.04.30 (Ludwig 2009). The 1σ external errors of $^{206}Pb/^{238}U$ ratios reported in the data table incorporate a ±1.0 % (±1.2% session 2) error in calibrating the standard zircon (see Stern and Amelin, 2003). No fractionation correction was applied to the Pb-isotope data; common Pb correction utilized the Pb composition of the surface blank (Stern, 1997). Isoplot v. 3.00 (Ludwig, 2003) was used to generate concordia plots and calculate weighted means. The error ellipses on the concordia diagrams, and the weighted mean errors are reported at 2σ.

Analyses of a secondary zircon standard (Fish Canyon Tuff – FCT and Temora 2) were interspersed between the sample analyses to verify the accuracy of the U-Pb calibration. Using the calibration defined by the z6266 standard, the weighted mean $^{206}Pb/^{238}U$ age of ten SHRIMP analyses of FCT zircon is 30.6±1.3 Ma (session1, 95% conf.) and 28.9 +/- 0.3 Ma (session2, 95% conf.). The accepted $^{206}Pb/^{238}U$ age of FCT is 28.402 +/- 0.023 Ma, based on 23 isotope dilution fractions (Schmitz and Bowring, 2001). Using the calibration defined by the z6266 standard, the weighted mean $^{206}Pb/^{238}U$ age of 7 SHRIMP analyses of Temora 2 zircon is 412.9±4.2 Ma (session 2, 95% conf.). The accepted $^{206}Pb/^{238}U$ age of Temora 2 is 416.5 +/-0.22 Ma, based on 21 isotope dilution fractions (Black et al., 2004).

For sample LA20, a total of 20 zircon areas were analyzed in two sessions. First session used a beam size of 15 μm, which introduced slightly high common/radiogenic Pb ratios. The only analyzed core has a ^{207}Pb corrected ^{206}Pb-^{238}U age of 310±5 Ma (Carboniferous) (Table A2). All 19 rims analyses define a regression line in a Tera-Wasserburg plot uncorrected for common Pb, with a lower intercept at 18.57±0.23 Ma and an upper intercept at 5188±170 Ma, similar to that defined by the estimated surface common Pb composition (Fig. 4b, Table A2) (MSWD = 1.8). All 11 spots from the second session yield an average ^{207}Pb corrected ^{206}Pb-^{238}U age of 18.5±0.2 Ma (MSWD = 2.07, common Pb anchored upper intercept) (Table A2), which we consider as the best age approximation for these rims.

For sample LA21, 18 spots were analyzed during the two sessions with the only core close to concordia with a 25.6±0.3 Ma ^{207}Pb corrected ^{206}Pb-^{238}U age (Table A2). Seventeen rim analyses define a regression line in a Tera-Wasserburg plot with a lower intercept at 18.61±0.25 Ma and an upper intercept at 5139±150 (MSWD = 1.8) (Fig. 4a, Table A2), again validating the common Pb correction. The results suggest the presence of a ~26 Ma inheritance and the magma crystallization at ~18.6 Ma, which is synchronous with the surrounding granite.

In zircon grains of sample LA60, the U contents of the areas away from zones with uraninite are very high, ranging from 2,900 to 12,700 ppm. It has been observed that ion probe analyses give systematically higher Pb/U ratios for zircon with U contents > 2000 ppm (Williams and Hergt, 2000). If uncorrected, this analytical matrix effect gives inaccurate old ages, for zircon with U contents ≥ 2000 ppm. In the case of LA60 the ^{207}Pb-corrected ^{206}Pb-^{238}U ages of zircon span from 16.3 to 18.9 Ma (Table A3), and show a strong linear correlation between ^{206}Pb-^{238}U age and U concentration (Figure 4c). This matrix affect was corrected by regressing the ^{206}Pb-^{238} U age against ^{238}U/^{96}Zr_2O, a measure of uranium concentration (MSWD = 2.6; n=6), and calculating the age at the intercept of the correlation line with the estimated concentration threshold for the matrix effect at 2000 ppm U. This treatment yields an age of 16.0 ± 0.6 Ma (6 meas., MSWD = 2.6 - 6 grains) (Fig. 4c, Table A2). This age is, interpreted as the time of crystallisation of the late dike.

A2 U/Pb ages of ganitoids within the Ksz.

Sample characteristics, age and location are listed in Table A1, samples from the Tangste area and gorge are located on Fig. 1b. Samples for which some information is lacking (e.g., Phillips, 2004, 2008) are listed in table A1 but not discussed below. Note that the various authors do not give the same names to the various plutons. We use the names given on Fig. 1 and Table A1.

A2-1Tangtse area (T Fig. 2).

The most spectacular outcrops of right-lateral mylonitic marbles, calcsilicates and orthogneiss are found on the Tangtse strand of the Ksz, around the Tangtse Gompa on the right bank of the Tangtse river (Fig. 1b; Fig. 3h, j). There, a mylonitised leucocratic dyke has been dated at 15.63±0.52 Ma (sample P11; ; Fig. 1b), while a dyke crosscutting the foliation yielded an age of 13.74±0.29 Ma (sample P8) (Phillips et al., 2004). This crosscutting dyke is syntectonic as it exhibits deformed tails compatible with right-lateral shear (see text). 2 km to the NE of Tangtse, zircons from the mylonitsed Tangtse leucogranite (Fig. 1b) yielded 6-8 ages spanning from 12 to 1221 Ma (n=39) with two dominant groups at 52-64 and particularly 15.2-20.9 Ma, the average of the 25 youngest being 18.0±0.6 Ma (sample 215 of Searle et al., 1988). The same body yielded a 6-8 age average age of 15.55±0.74 Ma for 1 zircon and 2 monazite concordant fractions (sample P1 of Phillips et al., 2004) (). Zircons from a nearby sample are 75.7±1 Ma old (sample R7 of Jain and Singh, 2008). Further NE along strike of the Tangtse strand, the Darbuk two micas granite is elongated parallel to the Ksz and shows an intensively sheared SW margin while its body is poorly deformed (Fig. 1b) (Jain and Singh, 2008). Zircons from this body have concordant rims with an average 6-8 age of 20.8±0.4 Ma and inherited core ages spanning from 45 to 671 Ma (sample SY46 of Jain and Singh, 2008) (). Much farther north along strike, near Satti (S Fig. 2a), zircons of a mylonitic leucogranite yield 6-8 ages spanning from 15.87±0.08 to 19 Ma (sample P38 of Phillips et al., 2004) comparable to the age of a nearby leucocratic dike with zircon rims at 15±0.4 Ma (sample 021 of Weinberg et al., 2000) (). Near Panamik (P, Fig. 2), a single Xenotime fraction from a cross-cutting dike has a 7-5 age of 13.73±0.34 while zircons 6-8 ages span from 18 to 26 Ma (P37, Phillips et al., 2004).

A2-2 Tangtse gorge (T Fig. 2).

Across strike from Tangtse, in the Tangtse gorge, zircons from the TMC have yielded several Cretaceous ages: 60.4±1.1Ma for leucogranitic dikes (sample SY26 of Jain and Singh, 2008), 70.5±0.6 Ma for the North Muglib pluton and 71.4±0.6 Ma for the South Muglib pluton (samples TNG131a and TNG62a of Reichardt et al., 2010), which have led some to propose that the main strike-slip deformation episode occurred between ~68 and ~75.7 Ma (Jain and Singh, 2008). However other zircons reveal much younger melting episodes. Yellowish zircons from migmatites give an average 6-8 age of 106±2.3Ma, but transparent zircons and overgrowth are much younger with a subgroup at 16.4±0.2 Ma and another in the 18-23 Ma range (sample 022 of Searle et al., 1988). In a Biotite granite, concordant ages span between 19.4±0.5 Ma and 69.2 Ma (sample SY25 of Jain and Singh, 2008), while another facies of the North Muglib pluton

yield 18±0.4 Ma (sample TNG148a of Reichardt et al., 2010).

A2-3 North Ayilari range (NA, Fig. 2a).

Along strike toward to the south, mylonites of the Ksz outcrop in the North Ayilari range (NA, Fig. 2a) (Lacassin et al., 2004; Matte et al., 1996). U/Pb ages of monazite and zircons in gneiss and syntectonic leucocratic dikes in the North Ayilari range (NA, Fig. 2a) have been interpreted has reflecting inheritance from several events spanning between the late Archean and the Jurassic but with two main magmatic events at 35–32 and 25–22 Ma followed by a period of metamorphism and metasomatism between 22 and 14 Ma (Valli et al., 2008). Field relationships indicate that sample C32 dated at 22.7±0.1Ma is synkinematic to the right-lateral shear, while the metamorphic event was interpreted as reflecting heat and fluid advection in the shear zone.

A2-4 Namru (N, Fig. 2a).

Only ~60km to the SE, near Namru (N on Fig. 2) the deformed granites show inherited zircon ages spanning from 2204 to 32 Ma but with most in the 52-46 and 35-32 intervals (Wang et al., 2009).

Tables

Table A1

Published U/Pb ages for granitoids in the Ksz. Zr, zircon; Mz, monazite; Xe, xenotime; Ti, titanite.

Table A2

Detailed U/Pb data for LA20, 21 and 60.

Appendix references :

Black, L.P., Kamo, S.L., Allen, C.M., Davis, D.W., Aleinikoff, J.N., Valley, J.W., Mundil, R., Campbell, I.H., Korsh, R.J., Williams, I.S., and Foudoulis, C., 2004, Improved 206Pb/238U microprobe geochronology by monitoring of a trace-element-related matrix effect; SHRIMP, ID-TIMS, ELA-ICP-MS and oxygen isotope documentation for a series of zircon standards.: Chemical Geology, v. 205, p. 115-140.

Jain, A.K., and Singh, S., 2008, Tectonics of the southern Asian Plate margin along the Karakoram Shear Zone: Constraints from field observations and U–Pb SHRIMP ages: Tectonophysics, v. 451, p. 186–205.

Lacassin, R., Valli, F., Arnaud, N., Leloup, P.H., Paquette, J.-L., Li, H., Tapponnier, P., Chevalier, M.-L., Guillot, S., Mahéo, G., and Xu, Z., 2004, Large-scale geometry, offset and kinematic evolution of the Karakorum fault, Tibet: Earth and Planetary Science Letters, v. 219, p. 255-269.

Matte, P., Tapponnier, P., Arnaud, N., Bourjot, L., Avouac, J.P., Vidal, P., Liu, Q., Pan, Y., and Wang, Y., 1996, Tectonics of WesternTibet between theTarim and the Indus: Earth and Planetary Science Letters, v. 142, p. 311 – 330.

Phillips, R.J., 2004, Macro- and micro-structural evolution of the Karakoram fault, NW Himalaya, University of Oxford.

—, 2008, Geological map of the Karakoram fault zone, Eastern Karakoram, Ladakh, NW Himalaya: Journal of Maps, p. 21-37.

Phillips, R.J., Parrish, R.R., and Searle, M.P., 2004, Age constraints on ductile deformation and long-term slip rates along the Karakoram fault zone, Ladakh: Earth and Planetary Science Letters, v. 226, p. 305-319.

Reichardt, H., Weinberg, R.F., Andersson, U.B., and Fanning, M.C., 2010, Hybridization of granitic magmas in the source: The origin of the Karakoram Batholith, Ladakh, NW India: Lithos, v. 116, p. 249-272.

Schmitz, M.D., and Bowring, S.A., 2001, U-Pb zircon and titanite systematics of the Fish Canyon Tuff: an assessment of high-precision U-Pb geochronology and its application to young volcanic rocks: Geochimica Et Cosmochimica Acta, v. 65, p. 2571-2587.

Searle, M.P., Weinberg, R.F., and Dunlap, W.J., 1988, Transpressional tectonics along the Karakoram fault zone, northern Ladakh: constraints on Tibetan extrusion, *in* Holdsworth, R.E., A., S.R., and Dewey , J.F., eds., Continental Transpressional and Transtensional Tectonics, Volume 135: Geol. Soc., London, Spec. Pub., p. 307-326.

Stern, R.A., 1997, The GSC Sensitive High Resolution Ion Microprobe (SHRIMP): analytical techniques of zircon U-Th-Pb age determinations and performance evaluation, *in* Canada, G.S.o., ed., Radiogenic Age and Isotopic Studies, Current Research 1997-F, Report, Volume 10, p. 1-31.

Stern, R.A., and Amelin, Y., 2003, Assessment of errors in SIMS zircon U-Pb geochronology using a natural zircon standard and NIST SRM 610 glass: Chemical Geology, v. 197, p. 111-146.

Valli, F., Leloup, P.H., Paquette, J.-L., Arnaud, N., Li, H., Tapponnier, P., Lacassin, R., Guillot, S., Liu, D., Deloule, E., Xu, Z., and Mahéo, G., 2008, New U-Th/Pb constraints on timing of shearing and long-term slip-rate on the Karakorum fault: Tectonics, v. 27.

Wang, S., Fang, X., Lai, Q., Zheng, D., and Wang, Y., 2009, New radiometric dating constrains the time for initiation of the Karakorum fault zone (KFZ), SW Tibet: Tectonophysics.

Weinberg, R.F., Dunlap, W.J., and Whitehouse, M., 2000, New field, structural and geochronological data from the Shyok and Nubra valleys, northern Ladakh: Linking Kohistan to Tibet, *in* Khan, M.A., Searle, M.P., and Jan, M.Q., eds., the Nanga Parbat Syntaxis and the Western Himalaya, Volume 170: Geol. Soc. London Spec. Pub., p. 253 – 275.

Williams, I.S., and Hergt, J.M., 2000, U-Pb dating of tasmanian dolerites: a cautionary tale of SHRIMP analysis of high-U zircon, *in* Woodhead, J.D., Hergt, J.M., and Noble, W.P., eds., New frontiers in Isotope Geoscience: Lorne.

Area	Locality	Sample	Rock type	Latitude (°'".")	longitude (°'".")	Mineral	Age (Ma)	± (Ma)	Reference
Nubra Valley	Sanstanling	P37	Croscutting leucogranite	34°38'11.02"N	7°39'15.66"E	Zr + Xe	13.73	0.34	Phillips et al., 2004
	Satti	P38	Mylonitic leucogranite	34°29'5.99"N	77°44'23.35"E	Zr	15.87	0.08	Phillips et al., 2004
	Satti	021	leucogranite	34°29'5.99"N	77°44'23.35"E	Zr	15.0	0.4	Weinberg et al., 2000
Darbuk	Darbuk leucogranite	SY46	S-type peraluminous 2 micas gneissose granite	34° 8'13.90"N	78° 6'7.10"E	Zr	20.8	0.4	Jain and Singh, 2008
		XX?				?	20.05	0.6	Phillips2004 - map-
		XX?				?	22.46	2.1	Phillips2004 - map-
Tangtse	Tangtse leucogranite	215	Mylonitic leucogranite	34° 2'19.99"N	78° 9'38.67"E	Zr	18.0	0.6	Searle et al., 1998
	Tangtse leucogranite	P1 (~215)	Mylonitic leucogranite	34°2'0.57"N	78°9'49.12"E	Zr, Mz, Xe	15.55	0.74	Phillips et al., 2004
	Tangtse Gompa	P11	Mylonitic leucogranite	34°01'28.21"N	78°12'05.88"E	Zr, Mz	15.63	0.52	Phillips et al., 2004
	Tangtse Gompa	P8	crosscuting dyke	34°01'32.5"N	78°10'26.10"E	Zr	13.72	0.18	Phillips et al., 2004
	Tangtse mylonite	R7	Tangtse mylonite	34°1'32.58"N	78°10'27.41"E	Zr	75.7	1	Jain and Singh, 2008
Tangtse gorge	Muglib granite	P46	Bt leucogranite	34°3'59.57"N	78°13'56.38"E	?	15.1	0.6	Phillips, 2004 (Ph.D)
	Muglib granite	XX?	pegmatitic dykes	34°3'59.57"N	78°13'56.38"E	?	12.72	0.04	Phillips, 2004 (Ph.D)
	near Muglib granite	P112	migmatitic melanosome	34°3'28.18"N	78°13'23.75"E	?	108	2	Phillips, 2004 (Ph.D)
	near Muglib granite	P113	tonalitic leucosome	34°3'28.18"N	78°13'23.75"E	?	17.31	0.13	Phillips, 2004 (Ph.D)
	Pangong Range	SY25	biotite granite gneiss	34° 2'14.80"N	78°12'47.64"E	Zr	68 - 51.5		Jain and Singh, 2008
	Pangong Range	SY25	biotite granite gneiss	34° 2'14.80"N	78°12'47.64"E	Zr	19.4	0.5	Jain and Singh, 2008
	Pangong Range	SY25	biotite granite gneiss	34° 2'14.80"N	78°12'47.64"E	Zr	69.2	1.3	Jain and Singh, 2008
	Pangong Range	SY26	leucogranite	34° 2'14.80"N	78°12'47.64"E	Zr	60.4	1.1	Jain and Singh, 2008
	Tangtse gorge	022	Migmatite	34° 2'46.54"N	78°13'30.97"E	Zr	17-20		Searle et al., 1998
	North Muglib pluton	TNG131a	Bt-granodiorite sheet	34°03'38.8"N	78°13'52.1"E	Zr	70.5	0.6	reichardt et al., 2010
	North Muglib pluton	TNG131a	Bt-granodiorite sheet	34°03'38.8"N	78°13'52.1"E	Ti	65.1	2.8	reichardt et al., 2011
	North Muglib pluton	TNG148a	Bt-leucogranite	34°03'40.4"N	78°13'52.7"E	Zr	18	0.4	reichardt et al., 2010
	North Muglib pluton	TNG148a	Bt-leucogranite	34°03'40.4"N	78°13'52.7"E	Ti	16.4	1.4	reichardt et al., 2010
Pangong Valley	NW of Pangong lake	P19	PMC Gt-St-Bt schist	33°58'8.49"N	78°22'38.79"E	MZ	108	0.6	Streule et al., 2009
	Near Muglib	TNG62a	South MuglibPluton	34°02'16.8"N	78°14'57.7"E	Zr	71.4	0.6	reichardt et al., 2010
	Near Muglib	XX?		34° 3'26.34"N	78°14'25.84"E	?	17.31	0.5	Phillips2004 - map-
NorthAyilari Range/ Zhaxikang	Ayilari Range section 1	L89	migmatitic gneiss	32°26'44.63"N	79°33'36.55"E	Mz (magmatic)	34.7	2.4	Valli et al., 2008
	Ayilari Range section 1	L89	migmatitic gneiss	32°26'44.63"N	79°33'36.55"E	Mz (magmatic)	23.4	4.0	Valli et al., 2008
	Ayilari Range section 1	L89	migmatitic gneiss	32°26'44.63"N	79°33'36.55"E	Zr (magmatic)	24.2	2.4	Valli et al., 2008
	Ayilari Range section 1	L89	migmatitic gneiss	32°26'44.63"N	79°33'36.55"E	Mz (metam)	18.2	1.8	Valli et al., 2008
NorthAyilari Range/ Gar	Ayilari Range section 2	P34	orthogneiss	32°25'00.40"N	79°42'06.10"E	Zr (metam)	22.1	4.7	Valli et al., 2008
	Ayilari Range section 3	P18	orthogneiss	32°23'28.9"N	79°43'35.0"E	Zr (magmatic)	34.4	1.3	Valli et al., 2008
	Ayilari Range section 3	P18	orthogneiss	32°23'28.9"N	79°43'35.0"E	Zr (magmatic)	23.3	4	Valli et al., 2008
	Ayilari Range section 3	P18	orthogneiss	32°23'28.9"N	79°43'35.0"E	Mz (magmatic)	25.2	1.6	Valli et al., 2008
	Ayilari Range section 3	P18	orthogneiss	32°23'28.9"N	79°43'35.0"E	Mz (metam)	18.8	2.8	Valli et al., 2008
	Ayilari Range section 3	P20	Gneiss	32°23'19.20"N	79°43'27.70"E	Zr (magmatic)	21.7	3.6	Valli et al., 2008
	Ayilari Range section 3	C32	Leucocratic dyke	32°23'17.60"N	79°43'25.30"E	Zr (magmatic)	32.5	2.6	Valli et al., 2008
	Ayilari Range section 3	C32	Leucocratic dyke	32°23'17.60"N	79°43'25.30"E	Zr (magmatic)	22.7	0.1	Valli et al., 2008
	Ayilari Range section 3	C32	Leucocratic dyke	32°23'17.60"N	79°43'25.30"E	Mz (metam)	15.8	0.2	Valli et al., 2008
	Ayilari Range section 4	C43	leuco orthogneiss	32°19'34.9"N	79°44'21.1"E	Zr (metam)	21.7	1.4	Valli et al., 2008
	Ayilari Range section 4	C43	leuco orthogneiss	32°19'34.9"N	79°44'21.1"E	Zr (metam)	17.8	4	Valli et al., 2008
	Ayilari Range section 4	C43	leuco orthogneiss	32°19'34.9"N	79°44'21.1"E	Mz (metam)	14.4	0.7	Valli et al., 2008
South Ayilari / Namru	Namru (main strand)	KK4	mylonitic granite?	31°53'58.16"N	80° 8'45.13"E	Zr	48		Wang et al., 2009
	Namru (main strand)	KK5	mylonitic granite?	31°53'58.16"N	80° 8'45.13"E	Zr	48		Wang et al., 2009
	Namru (main strand)	KK9	mylonitic granite?	31°53'58.16"N	80° 8'45.13"E	Zr	46.4-51.7		Wang et al., 2009
	Namru (main strand)	KK9	mylonitic granite?	31°53'58.16"N	80° 8'45.13"E	Zr	37-45		Wang et al., 2009
	Namru (main strand)	KK9	mylonitic granite?	31°53'58.16"N	80° 8'45.13"E	Zr	32-34		Wang et al., 2009
	Namru (South strand)	KK3	dyke	31°53'28.66"N	80° 5'59.07"E	Zr	65.7-2204		Wang et al., 2009
	Namru (South strand)	KK3	dyke	31°53'28.66"N	80° 5'59.07"E	Zr	31.7 - 35.1		Wang et al., 2009

Table A1

SAMPLE							ATOMIC RATIOS								204 CORRECTED (1)					207 CORRECTED (2)		AGES			
																						204 corrected		207 corrected	
Spot Name	**Session**	**Beam location**	**U (ppm)**	**Th/U**	**206* (ppm)**	**f206(207)%**	**204Pb/206Pb**	**%err**	**208Pb/206Pb**	**%err**	**238U/206Pb**	**%err**	**207Pb/206Pb**	**%err**	**207*Pb/235U**	**%err**	**206*Pb/238U**	**%err**	**Err Corr**	**206*Pb/238U**	**%err**	**206Pb/238U Age**	***1s err***	**206Pb/238U Age**	***1s err***
LA20																									
9986-17.1	1	core	1263	0,06	5,3	14,55	1,2E-3	23	0,084	8,1	339	1,2	0,0559	2,8	0,044	45	0,00414	4,3	0,10	0,0029	1,3	**26,6**	*1*	**25,6**	*0,3*
9986-17.2	1	rim/ cristal	1765	0,31	8,0	20,50	8,2E-4	35	0,081	7,3	331	1,2	0,0630	3,1	0,012	114	0,00275	4,2	0,04	0,0030	1,3	**17,7**	*0,7*	**18,0**	*0,3*
9986-1.1	2	rim/ cristal	3117	0,264	5,4	1,42	1,9E-3	23	0,096	5,1	335	1,4	0,0636	6,2	0,0210	9	0,00298	1,3	0,14	0,0029	1,5	**19,2**	*0,3*	**19,1**	*0,2*
9986-10.1	2	rim/ cristal	1751	0,335	5,2	1,67	6,4E-4	89	0,117	6,4	338	1,2	0,0669	2,0	0,0198	12	0,00290	1,6	0,13	0,0029	1,3	**18,7**	*0,3*	**18,6**	*0,3*
9986-11.1	2	rim/ cristal	1731	0,361	6,9	2,24	1,0E-3	26	0,114	6,0	301	1,2	0,0590	5,3	0,0189	13	0,00284	1,4	0,11	0,0033	1,3	**18,3**	*0,3*	**18,2**	*0,2*
9986-14.1	2	rim/ cristal	2117	0,324	4,2	2,08	1,3E-3	31	0,096	5,9	344	1,3	0,0671	2,1	0,0152	12	0,00289	1,3	0,11	0,0028	1,3	**18,6**	*0,2*	**18,8**	*0,2*
9986-18.1	1	rim/ cristal	2380	0,40	3,8	15,13	1,7E-3	31	0,131	6,7	331	1,2	0,0702	6,7	0,016	59	0,00292	3,0	0,05	0,0029	1,4	**18,8**	*0,6*	**19,0**	*0,3*
9986-18.2	2	rim/ cristal	1501	0,390	2,5	3,01	1,2E-3	96	0,109	9,0	331	1,3	0,0876	4,2	0,0180	21	0,00293	1,6	0,07	0,0029	1,4	**18,9**	*0,3*	**18,9**	*0,3*
9986-19.1	1	rim/ cristal	1671	0,34	4,3	21,01	2,6E-3	23	0,097	7,5	347	1,2	0,0763	2,0	0,013	114	0,00285	4,3	0,04	0,0028	1,3	**18,3**	*0,8*	**18,6**	*0,3*
9986-19.2	2	rim/ cristal	980	0,421	3,9	2,12	1,8E-3	24	0,190	6,9	339	1,2	0,0648	3,1	0,0286	25	0,00296	2,4	0,10	0,0029	1,3	**19,0**	*0,5*	**18,5**	*0,3*
9986-2.1	2	rim/ cristal	2190	0,309	5,4	3,23	9,8E-3	14	0,077	5,7	287	1,1	0,205	2,3	0,0143	22	0,00289	1,6	0,07	0,0028	1,3	**18,6**	*0,3*	**18,8**	*0,3*
9986-20.1	1	rim/ cristal	1749	0,27	6,3	14,80	6,7E-3	19	0,232	7,3	296	2,0	0,170	2,5	0,024	52	0,00287	3,9	0,08	0,0029	2,1	**18,5**	*0,7*	**18,2**	*0,2*
9986-20.2	2	rim/ cristal	1820	0,318	12,2	4,56	4,4E-3	20	0,077	10,3	259	1,0	0,135	1,9	0,0141	26	0,00275	1,7	0,06	0,0035	1,1	**17,7**	*0,3*	**17,9**	*0,2*
9986-21.2	2	rim/ cristal	1604	0,272	5,3	3,12	6,0E-3	20	0,093	6,5	332	1,3	0,124	3,0	0,0150	19	0,00286	1,5	0,08	0,0027	1,4	**18,4**	*0,3*	**18,6**	*0,2*
9986-5.1	2	rim/ cristal	2060	0,352	4,5	1,11	8,4E-3	24	0,126	6,0	207	1,1	0,196	2,7	0,0232	15	0,00292	1,6	0,11	0,0040	1,3	**18,8**	*0,3*	**18,6**	*0,2*
9986-6.1	1	rim/ cristal	2183	0,36	4,2	16,93	1,2E-2	16	0,157	6,3	289	1,1	0,208	2,7	0,026	38	0,00289	3,1	0,08	0,0028	1,4	**18,6**	*0,6*	**18,2**	*0,2*
9986-7.1	1	rim/ cristal	2464	0,33	6,0	11,61	8,7E-3	15	0,128	7,2	291	1,4	0,169	2,5	0,031	29	0,00298	3,2	0,11	0,0029	1,5	**19,2**	*0,6*	**18,6**	*0,4*
9986-8.1	1	rim/ cristal	1829	0,31	4,3	16,36	8,5E-3	22	0,086	7,9	296	1,1	0,185	2,9	0,016	70	0,00284	3,5	0,05	0,0028	1,3	**18,3**	*0,6*	**18,4**	*0,2*
LA21b																									
9988-20.2	1	core	206	0,19	4,1	6,07	7,0E-3	21	0,100	8,4	314	1,1	0,140	3,4	0,515	16	0,05049	2,0	0,12	0,0028	1,3	**318**	*6*	**310**	*5*
9988-1.1	1	rim/ cristal	1692	0,33	3,0	12,10	1,3E-2	23	0,012	10,5	267	1,2	0,258	4,3	0,014	71	0,00280	3,0	0,04	0,0028	2,1	**18,0**	*0,5*	**18,3**	*0,2*
9988-11.1	2	rim/ cristal	2603	0,262	3,7	1,11	8,6E-3	34	0,090	6,0	305	1,1	0,162	3,5	0,0209	7	0,00294	1,3	0,20	0,0028	1,3	**18,9**	*0,2*	**18,8**	*0,2*
9988-14.1	1	rim/ cristal	1533	0,22	4,2	14,96	8,1E-3	19	0,084	9,7	306	1,1	0,161	3,1	0,013	156	0,00278	6,0	0,04	0,0028	1,3	**17,9**	*1*	**18,2**	*0,2*
9988-16.1	1	rim/ cristal	1730	0,33	4,8	14,03	6,0E-3	20	0,039	9,2	310	1,1	0,139	3,1	0,016	66	0,00281	3,3	0,05	0,0029	1,2	**18,1**	*0,6*	**18,2**	*0,2*
9988-19.1	1	rim/ cristal	1941	0,34	6,1	10,41	4,1E-3	23	0,094	9,2	308	1,0	0,114	6,3	0,021	40	0,00289	2,6	0,07	0,0030	1,4	**18,6**	*0,5*	**18,5**	*0,2*
9988-2.1	2	rim/ cristal	2183	0,296	8,9	1,15	3,5E-3	21	0,118	5,9	19	1,4	0,124	2,6	0,0198	10	0,00291	1,3	0,14	0,0492	1,5	**18,7**	*0,3*	**18,7**	*0,2*
9988-20.1	1	rim/ cristal	2367	0,33	6,7	7,09	6,3E-3	22	0,079	14,3	315	1,3	0,122	2,8	0,023	31	0,00301	2,1	0,07	0,0029	1,4	**19,4**	*0,4*	**19,2**	*0,3*
9988-21.1	1	rim/ cristal	2748	0,43	4,4	10,97	2,1E-2	10	0,088	7,7	169	2,3	0,331	1,9	0,010	88	0,00282	3,0	0,03	0,0039	2,6	**18,2**	*0,5*	**18,6**	*0,3*
9988-22.1	2	rim/ cristal	1924	0,253	5,9	6,77	6,8E-3	22	0,034	6,0	290	2,1	0,197	3,4	0,0125	31	0,00288	1,7	0,06	0,0028	2,3	**18,5**	*0,3*	**18,9**	*0,3*
9988-25.1	2	rim/ cristal	2273	0,350	6,6	1,43	1,5E-3	21	0,116	5,7	349	1,2	0,0655	2,4	0,0180	21	0,00293	1,7	0,08	0,0028	1,3	**18,8**	*0,3*	**18,9**	*0,2*
9988-26.1	2	rim/ cristal	2030	0,310	4,3	2,68	1,8E-3	22	0,092	5,9	342	1,3	0,0781	2,4	0,0156	14	0,00289	1,4	0,10	0,0028	1,3	**18,6**	*0,3*	**18,8**	*0,2*
9988-28.1	2	rim/ cristal	2127	0,306	4,5	2,94	1,2E-3	68	0,119	5,3	335	1,2	0,0626	3,0	0,0197	24	0,00282	1,9	0,08	0,0029	1,3	**18,2**	*0,3*	**18,1**	*0,2*
9988-30.1	1	rim/ cristal	2274	0,33	4,0	11,85	1,8E-3	19	0,277	9,2	340	1,4	0,0672	3,0	0,043	24	0,00304	3,6	0,15	0,0029	1,4	**19,6**	*0,7*	**18,2**	*0,4*
9988-4.1	2	rim/ cristal	2749	0,313	6,6	2,59	6,4E-4	33	0,085	5,3	337	1,2	0,0609	1,8	0,0167	12	0,00279	1,4	0,12	0,0029	1,2	**18,0**	*0,2*	**18,0**	*0,2*
9988-5.1	2	rim/ cristal	1784	0,332	4,8	3,16	3,9E-3	15	0,085	8,8	324	1,3	0,0900	1,9	0,0201	13	0,00283	1,5	0,12	0,0029	1,3	**18,2**	*0,3*	**18,1**	*0,2*
9988-6.1	2	rim/ cristal	1575	0,374	9,7	3,97	5,1E-4	30	0,119	5,8	291	1,2	0,0533	1,5	0,0160	30	0,00282	1,7	0,06	0,0034	1,2	**18,2**	*0,3*	**18,3**	*0,3*
9988-7.1	1	rim/ cristal	1225	0,23	5,7	22,97	8,3E-4	75	0,310	8,1	337	1,3	0,0568	2,0	0,027	85	0,00289	6,9	0,08	0,0029	1,3	**18,6**	*1*	**18,1**	*0,4*
9988-8.1	2	rim/ cristal	1790	0,227	5,0	2,06	1,5E-3	23	0,081	7,0	337	1,2	0,0619	2,1	0,0182	27	0,00292	1,9	0,07	0,0029	1,3	**18,8**	*0,4*	**18,8**	*0,2*
9988-9.1	2	rim/ cristal	1641	0,373	5,2	3,14	1,7E-3	48	0,106	6,0	344	1,2	0,0755	2,6	0,0159	14	0,00285	1,5	0,11	0,0028	1,3	**18,3**	*0,3*	**18,5**	*0,3*
LA60																									
9994-14.1	1	rim/ cristal	12688	0,03	6,3	3,35	9,7E-3	15	0,009	7,6	340	1,1	0,168	2,6	0,019	10	0,00291	1,1	0,11	0,0025	1,2	**18,8**	*0,2*	**18,7**	*0,2*
9994-17.1	1	rim/ cristal	3582	0,03	8,0	14,19	8,2E-3	15	0,009	7,3	330	1,1	0,172	2,2	0,019	42	0,00260	2,8	0,07	0,0026	1,2	**16,7**	*0,5*	**16,6**	*0,2*
9994-2.1	1	rim/ cristal	2974	0,03	12,9	16,74	4,4E-3	17	-0,028	7,8	373	1,0	0,087	3,7	0,007	127	0,00245	3,2	0,03	0,0026	1,1	**15,8**	*0,5*	**16,3**	*0,2*
9994-20.1	1	rim/ cristal	9440	0,03	23,7	6,58	3,8E-3	12	-0,005	6,5	320	1,0	0,097	1,7	0,017	19	0,00292	1,3	0,07	0,0029	1,0	**18,8**	*0,3*	**18,9**	*0,2*
9994-3.1	1	rim/ cristal	6057	0,03	14,8	7,56	3,0E-3	22	-0,002	8,7	350	1,4	0,111	2,2	0,007	63	0,00248	1,8	0,03	0,0026	1,4	**16,0**	*0,3*	**16,4**	*0,2*
9994-4.1	1	rim/ cristal	6358	0,05	6,4	5,22	8,4E-3	19	0,095	7,0	332	1,6	0,173	2,6	0,025	15	0,00270	1,8	0,12	0,0026	1,8	**17.4**	*0,3*	**17,0**	*0,2*
9994-6.1	1	rim/ cristal	2912	0,03	31,7	14,55	1,9E-3	15	0,078	7,4	332	1,0	0,075	1,7	0,018	56	0,00257	3,6	0,06	0,0029	1,0	**16,6**	*0,6*	**16,5**	*0,3*

Spot name follows the convention x-y.z; where x = sample number, y = grain number and z = spot number. Multiple analyses in an individual spot are labelled as x-y.z.z
Uncertainties reported at 1s and are calculated by using SQUID 2.22.08.04.30, rev. 30 Apr 2008
$f206_{207}$ refers to mole fraction of total 206Pb that is due to common Pb, calculated using the 207Pb-method; common Pb composition used is the surface blank (4/6: 0.05770; 7/6: 0.89500; 8/6: 2.13840)
* refers to radiogenic Pb (corrected for common Pb) (1) based on 204 method; (2) based on 207 method
Discordance relative to origin = 100 * ((207/206 age -206/238 age)/(207Pb/206Pb age))
Calibration standard 6266; U = 910 ppm; Age = 559 Ma; 206Pb/238U = 0.09059
2 sessions have been runned: session 1 -beam size 13x16um
Error in $^{206}Pb/^{238}U$ calibration 1.0% (included)
Standard Error in Standard calibration was 0.30% (not included in above errors but required when comparing data from different mounts).
Session 2 -beam size 17x23um
Error in $^{206}Pb/^{238}U$ calibration 1.23% (included)
Standard Error in Standard calibration was 0.39% (not included in above errors but required when comparing data from different mounts).

Table A2